




## Article

# Effectiveness of Tuned Mass Damper in Reducing Damage Caused by Strong Earthquake in a Medium-Rise Building

Lucas Mazzon , Giada Frappa  and Margherita Pauletta 

Polytechnic Department of Engineering and Architecture, University of Udine, Via delle Scienze, 206, 33100 Udine, Italy; giada.frappa@uniud.it (G.F.); margherita.pauletta@uniud.it (M.P.)

\* Correspondence: mazzon.lucas@spes.uniud.it

**Abstract:** A case study where a tuned mass damper (TMD) was installed at the top of a five-story reinforced concrete (RC) building is presented. The aim of the study was to investigate the effectiveness of the TMD in changing the structural behavior of medium-rise existing buildings from dissipative to non-dissipative in order to eliminate reparation or demolition costs resulting from damages caused by strong earthquakes. The TMD mass is made by a RC slab lying on flat surface sliders. Horizontal stiffness and damping of the TMD are both provided by lead rubber isolators in the first proposed solution and by low-damping rubber isolators and viscous linear dampers, respectively, in the second. The improvement in the building's structural behavior attained with the installation of the TMD was assessed by considering the flexural demand over capacity ratios of structural elements and the energy dissipated by the TMD. These results are compared with those of the same building retrofitted with a base isolation system. In both of the proposed solutions, TMD remarkably changed the modal behavior of the considered building, improved the flexural verifications, and dissipated most of the input seismic energy. It is therefore demonstrated that a TMD is a valid solution for the retrofit of medium-rise existing buildings.

**Keywords:** tuned mass damper; passive energy dissipation; medium-rise building; RC structure; non-dissipative structure; seismic isolation; retrofit of existing building; earthquake



**Citation:** Mazzon, L.; Frappa, G.; Pauletta, M. Effectiveness of Tuned Mass Damper in Reducing Damage Caused by Strong Earthquake in a Medium-Rise Building. *Appl. Sci.* **2023**, *13*, 6815. <https://doi.org/10.3390/app13116815>

Academic Editor: Maria Favvata

Received: 15 May 2023

Revised: 30 May 2023

Accepted: 2 June 2023

Published: 4 June 2023



**Copyright:** © 2023 by the authors. Licensee MDPI, Basel, Switzerland. This article is an open access article distributed under the terms and conditions of the Creative Commons Attribution (CC BY) license (<https://creativecommons.org/licenses/by/4.0/>).

## 1. Introduction

Tuned mass dampers (TMDs) are mechanical systems that are widely used to reduce the amplitude of dynamic vibrations transmitted by the support to machines or structures in order to guarantee their correct functioning or avoid damages. In the field of construction, a TMD is usually placed on the top floors or on the rooftop of buildings to reduce their swaying due to wind forces. However, the seismic response of buildings can also benefit from TMDs [1,2], as they can be used as passive supplemental energy dissipation devices. In this case, the TMD frequency is designed to be tuned with the frequency of the main vibrational mode of the building in order to resonate out of phase with the building structure. Therefore, the effects of the main vibrational mode of the building during seismic behavior are mitigated, and the inertial forces arising in the structural members due to seismic forces are reduced.

In analytical applications, the mechanical behavior of TMDs is represented by a mass connected to the main structure by a spring and a dashpot arranged in parallel. In this schematization, the TMD's behavior is described by its mass, frequency and damping, which are designed on the basis of the main vibration modes of the building. In these applications, the TMD can be any device that behaves like such a system, e.g., a pendulum with dampers or a concrete slab on rubber isolators.

In the literature, several TMD design methods exist [3–34]. Among these, those developed in the last 15 years [9–34] propose advanced procedures aiming to optimize the TMD design in order to obtain the highest benefits regarding the seismic response of the

building. The most recent design methods either provide formulas coming from closed-form solutions of mechanical models [10–24] or consist of genetic algorithms that output the best design parameters [25–31]. All these methods focus on the optimization of one or more control parameters characterizing the seismic response of the building equipped with the TMD, e.g., the minimization of the highest floor acceleration or displacement or the maximization of energy dissipated by the TMD. The effectiveness of the design method in reducing the internal forces in structural members is fundamental and depends both on the loads considered in the design process and on the chosen control parameter. Actually, an inadequate design due to, for example, neglecting the soil–structure interaction effects on the building in the TMD design [21], can cause the plasticization of some structural members, leading to a decrease in the vibration mode frequencies. As a consequence, the resonance between the TMD and the building’s main vibrational modes vanishes, and a detuning of the TMD occurs. Detuning conditions can also arise during the building’s lifespan due to variations in the parameters affecting the vibration frequencies. This occurs when an increase in the building mass or a change in the stiffness occurs due to degradation of the rubber layers in seismic isolators.

Since a correctly designed TMD can remarkably improve the behavior of the structure under horizontal loads, several applications to different types of structures, such as tall buildings, skyscrapers, bridges and wind turbines [35,36], have been studied by researchers. However, only a few applications of TMD to existing buildings for their seismic retrofit have been found. These include: the installation of TMD on the top of multi-story buildings sited in Armenia (Assatourians A. and Mehrdoust M. [37]) to reduce the base shear and the top floor displacements; the roof substitution of the city tower in Rieti, Italy, including a TMD, to increase the vibrational periods and limit the displacements’ amplitude of the tower (Clemente P. [38]); the application of a TMD on the top of a 13-story building to reduce structural and non-structural damage (Villaverde R. [39]); the modification of the penthouses of ten buildings in order to make them act as masses of TMDs to reduce the overall seismic demand on structural members (Johnson J. et al. [40]). Such a limited use of TMDs in the retrofit of existing buildings is probably due to the increase in the building’s total mass and, thus, gravity loads.

In this paper, a case study where a TMD is installed at the top of a medium-rise reinforced concrete (RC) building is presented. The building structure without the TMD was initially designed with dissipative behavior in accordance with the Italian Building Code [41]. The aim of the TMD application is to modify the structural behavior of the building from dissipative to non-dissipative in order to eliminate reparation or demolition costs after a strong seismic event. In the considered case study, the mass of the TMD was made by an RC slab lying on flat surface sliders (FSSs). Two different solutions are proposed to provide horizontal stiffness and damping to the added system. One involves the use of rubber isolators (RIs), which replace some of the FSSs installed along the perimeter of the roof. The other is based on the use of low = damping rubber isolators (LDRIs) and viscous linear dampers (VLDs) installed along the roof perimeter, together with the FSSs. The design of the TMD was performed in accordance with the procedure described by Christopoulos in [5]. The effects of the TMD application on the internal forces arising in the structural members will be discussed in comparison with those acting in the original building (OB). The improvement in the building’s structural behavior provided by the TMD is assessed on the basis of the flexural demand over capacity ratios and the energy dissipated by the TMD.

## 2. Case Study

The case study is a six-story residential building located in Tolmezzo, Italy. The building plan is rectangular with dimensions of 18.15 m × 11.90 m (Figure 1) and is the same for all five floors. The interstory height is 3.00 m, except for the ground floor, which is 3.30 m high. The bearing structure against seismic actions is made by RC walls placed along the building perimeter (walls S1–S6 in Figure 2) and on the sides of the stairwell and the eleva-

tor shaft parallel to the Y direction (S7–S8 and A1–A2 in Figure 2). The resistance against vertical loads is provided by both walls and columns (P1–P9 in Figure 2). Columns and walls are connected at floor level by beams oriented along the building’s main directions (X and Y in Figure 1), following the dotted grid in Figure 2. Walls S7–S8, A1–A2 rise above the flat rooftop, as shown in Figure 3, to allow the access to the roof and the housing of the elevator technical compartment. According to the dimensions shown in Figures 1 and 3, the slenderness of the building is calculated as the ratio between the building’s height and the width of its base, which is equal to approximately 1 in the X direction and 1.5 in the Y direction. A building can be considered a skyscraper if this ratio is at least almost 10. Hence, the considered case study falls in the range of medium- or even low-rise buildings. The cross-sections of vertical elements stay the same for all the stories; only the walls’ longitudinal reinforcements are reduced from the fourth floor upward, where steel bars of diameter  $\phi 20$  change to  $\phi 16$ . The dimensions of structural members cross-sections are shown in Table 1. The reinforcement layouts at the base of vertical elements are shown in Figure 4. Floors are made by RC joists with a depth of 20 cm, a 5 cm thick RC slab at the top, and hollow bricks as lightening elements. The building foundations are made of a RC slab with dimensions of 19.15 m  $\times$  12.90 m  $\times$  0.80 m. The materials used for the building design are concrete of Italian grade C35/45, with characteristic compressive strength  $f_{ck} = 35$  MPa and Young’s modulus  $E_c = 34$  GPa, and reinforcing steel of Italian grade B450C, with characteristic yield strength  $f_{yk} = 450$  MPa and Young’s modulus  $E_s = 210$  GPa. Both concrete and steel are assumed to be linear materials in the finite element model of the building.

**Table 1.** Cross-sections of structural members and type of finite element used for their modeling.

Element	Type	Section	Finite Element
P1-9	Column	0.55 m $\times$ 0.55 m	Frame
S1-4	Wall	0.30 m $\times$ 3.80 m	Shell
S5-8	Wall	0.30 m $\times$ 3.40 m	Shell
A1-2	Wall	0.30 m $\times$ 2.10 m	Shell
(Beams)	Beam	0.25 m $\times$ 0.50 m	Frame

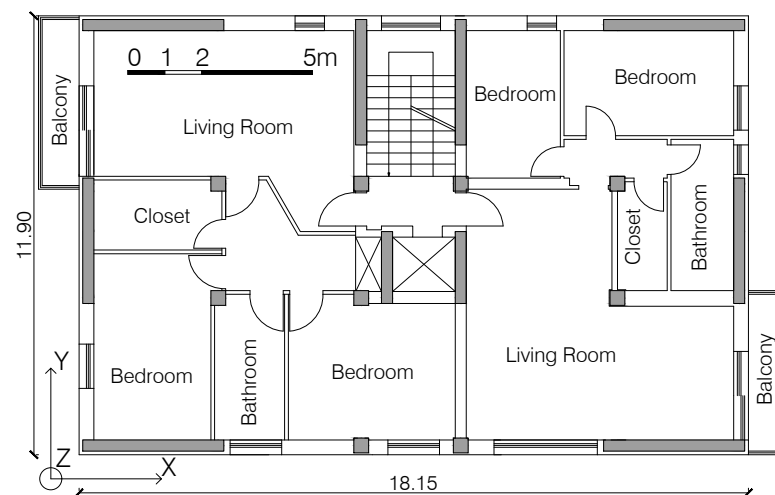


**Figure 1.** Plan of the typical building floor.

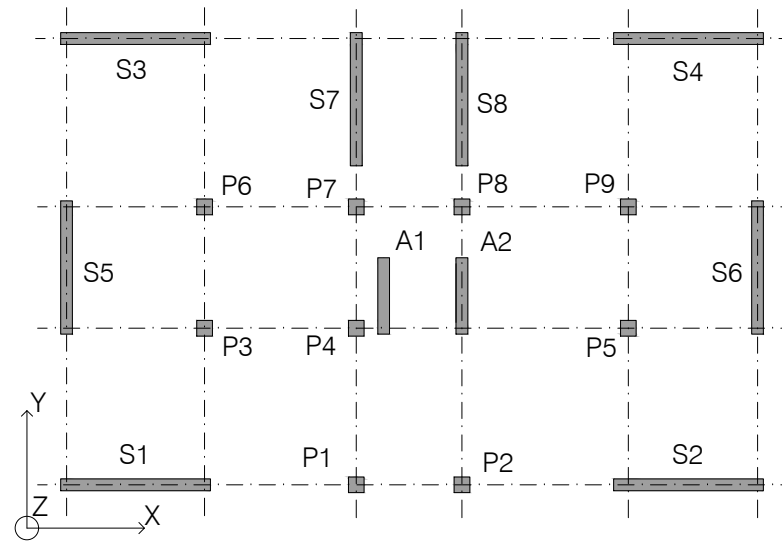


Figure 2. Plan view of vertical structural elements.

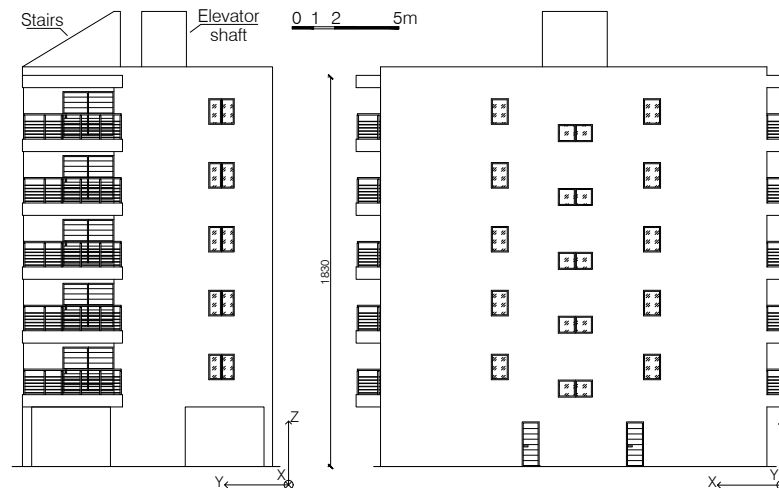


Figure 3. Building elevation in X direction on the left, and Y direction on the right.

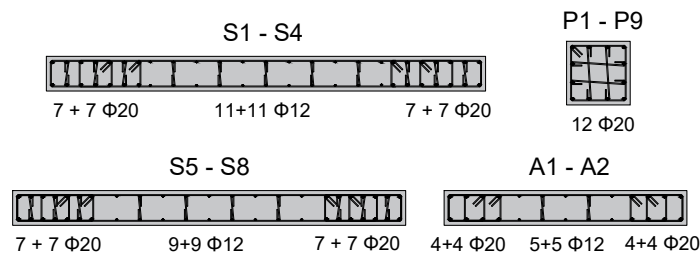


Figure 4. Reinforcement layouts in vertical structural elements at the ground floor.

The design of the RC structure against seismic actions was performed according to the dissipative behavior required by the Italian Building Code [41] for ductile wall structures, corresponding to a behavior factor  $q = 3$ . The finite element model (FEM) of the building was made using the software SAP2000 [42]. Beams and columns were modeled through frame elements, while shell elements were used for wall modeling (Table 1). Floors were assumed to behave as rigid diaphragms. The effects of cracking on structural members were taken into account by reducing the shear and flexural stiffnesses of cross-sections by 20% for vertical elements and by 50% for beams. The considered cracking is mainly due to the vertical loads for beams and to the horizontal loads for columns. In no case were

these cracks considered to be connected to a non-linear behavior of the structural elements, which are assumed to still be subjected to elastic deformations even after cracking.

Gravity loads per unit area applied to the FEM of the building are resumed in Table 2, where  $g_{1,k}$  and  $g_{2,k}$  are the permanent structural and non-structural characteristic loads, respectively, and  $q_k$  is the characteristic variable load. A distributed load of 5.6 kN/m was applied to the perimeter beams to consider the self-weight of masonry external infills. The self-weight and self-mass of structural elements were calculated by the software on the basis of their geometric and material properties. The FEM analyses are performed considering the load combinations at the ultimate limit state (ULS) provided by [41] for static and seismic load conditions. For the seismic analyses, the life-safety limit state, in Italian “Stato Limite di salvaguardia della Vita” (SLV), is considered herein. The seismic action was determined considering a building design service life of 50 yr and a ground of type *B*, which involves a return period of the seismic actions of 475 yr. In the following, the ULS acronym is used to indicate the static load combination of actions.

**Table 2.** Gravity loads per unit area.

	$g_{1,k}$ [kN/m <sup>2</sup> ]	$g_{2,k}$ [kN/m <sup>2</sup> ]	$q_k$ [kN/m <sup>2</sup> ]
Floor	3.5	2.7	2.0
Balcony	3.5	2.7	4.0
Rooftop	3.5	1.5	2.0
Stairs	4.3	1.0	4.0

Table 3 shows the periods and the participating mass ratios of the most significant modes of the OB, i.e., the modes having a participating mass ratio greater or equal to 5% and that, globally, provide a mass participating ratio  $\geq 85\%$  in each main direction.  $T_i$  indicates the period of the  $i$ -th mode, and  $\alpha_{i,j}$  indicates the participating mass ratio of the  $i$ -th mode in  $j$  direction. The values of the participating mass ratio in  $j$  direction which contributes the most for each mode are underlined in Table 3.

**Table 3.** Periods and mass participating ratios of the most significant modes of OB.

Mode $i$	$T_i$	$\alpha_{i,X}$	$\alpha_{i,Y}$	$\alpha_{i,Rz}$	$\Sigma \alpha_{i,X}$	$\Sigma \alpha_{i,Y}$	$\Sigma \alpha_{i,Rz}$
1	0.39 s	<u>66.3%</u>	0.1%	1.0%	66.3%	0.1%	1.0%
2	0.37 s	0.2%	<u>68.3%</u>	0.0%	66.5%	68.4%	1.1%
3	0.34 s	1.0%	0.2%	<u>66.0%</u>	67.5%	68.6%	67.1%
4	0.08 s	0.1%	<u>18.7%</u>	0.0%	67.6%	87.3%	67.1%
5	0.08 s	<u>14.8%</u>	0.1%	0%	82.4%	87.4%	67.1%
6	0.07 s	3.4%	0.0%	<u>6.4%</u>	85.8%	87.4%	73.5%
7	0.07 s	2.0%	0.0%	<u>13.4%</u>	87.8%	87.4%	86.9%

A fast non-linear analysis was performed. This is a modal analysis method, implemented by SAP2000, designed to be used for structural systems that are primarily linear elastic but that only have a limited number of predefined non-linear elements. FNA is well-suited for time-history analysis, which is the analysis used in the case study, because of its computationally efficient formulation. This efficiency is due to the separation of the non-linear-objects vector from the elastic stiffness matrix and the damped equations of motions. At each time increment, forces within the non-linear-objects vector are resolved through an iterative process, while the uncoupled modal equations are solved exactly. This allows the formulation to rapidly converge to the equilibrium solution. Regarding the considered case study, the only non-linear members are the devices used to reproduce the stiffness and the dissipation properties of the TMD, which are specified in the following section. Hence, FNA is a suitable analysis method for the case study. The ground motion is modeled using three different artificial accelerograms acting simultaneously along the horizontal directions *X* and *Y* and the vertical direction *Z*. Three independent analyses

were conducted, considering different ground motions. The accelerograms were generated by the software SIMQKE\_GR [43], matching their spectrum with the site elastic response spectrum provided by the Italian Code for a 5% damping coefficient, which is shown in Figure 5. The 5% damping factor takes account of all phenomena related to the building shaking under horizontal loads contributing to energy dissipation in elastic conditions, such as concrete viscous properties and cracking. The accelerograms have a stationary part that starts at time  $t = 2$  s and lasts 10 s, for a total duration of 30 s. One of the horizontal accelerograms used in the analyses is shown in Figure 6. The accelerometer record presented in Figure 6 refers to the life-safety limit state according to the Italian Building Code [41], hence with a 10% probability of occurrence in 50 years. The construction site of the building, Tolmezzo, is located in one of the areas of Italy with the highest seismicity. Therefore, the accelerogram shown is one of the most demanding for the Italian territory. For the structural members' design, the most disadvantageous internal forces obtained from the three analyses are considered.

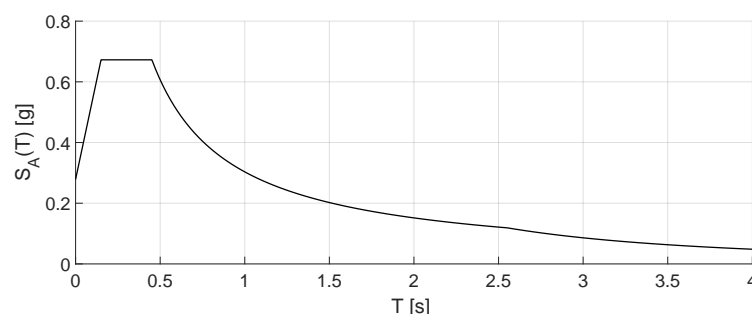


**Figure 5.** Site elastic response spectrum for the horizontal acceleration component according to [41].

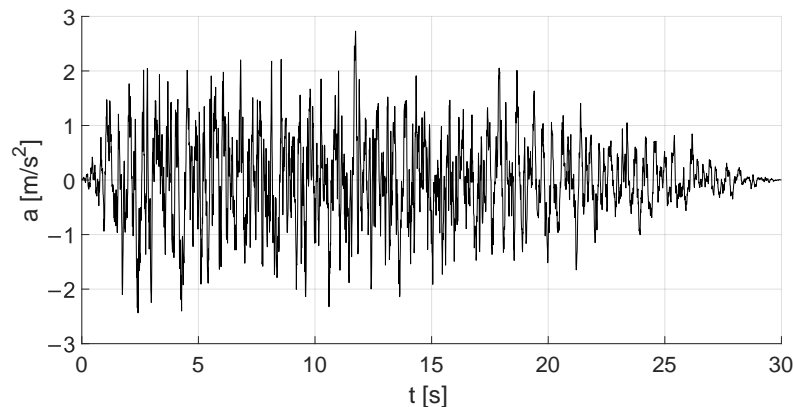


**Figure 6.** Horizontal accelerogram used in one of the seismic analyses of the building.

### 3. TMD Design Method

The mass of the TMD constituted a RC slab, 19.65 m long and 13.40 m wide, overlooking the entire rooftop and protruding by about 1 m from each façade, as shown in Figure 7. The slab thickness was constant, and it was assumed as a design parameter of the TMD mass. A steel structure composed of braced frames oriented in the  $X$  and  $Y$  directions was installed on the rooftop to support the TMD above the stairwell and the elevator shaft, as shown in Figure 8. The RC slab lay on flat surface sliders (FSSs) anchored to the beam–column joints of the steel structure, which allowed the RC slab to sway out of phase with the building. The correct disposition of LRIs, LDRI and VLDs in the two proposed solutions will be described in the design process in the next section.

In the steel structure, horizontal (Figure 7) and vertical braces (Figure 8) were used to provide in-plane stiffness to the plane at the base of the FSSs and horizontal stiffness to the steel frame, respectively. The steel structure's self-weight is negligible in comparison

with that of the building. Therefore, the increase in the building’s seismic mass due to this structure is also negligible. The design of the TMD was performed taking into account the availability of a new external living space at the level of the original roof and, consequently, the increase in gravity loads due to the variation in the roof’s intended use. In the FEM of the building, the steel structure was modeled through frame elements, while the RC slab was modeled through shell elements. For the FSS modeling, non-linear link elements of ‘Friction Isolator’ type were used.

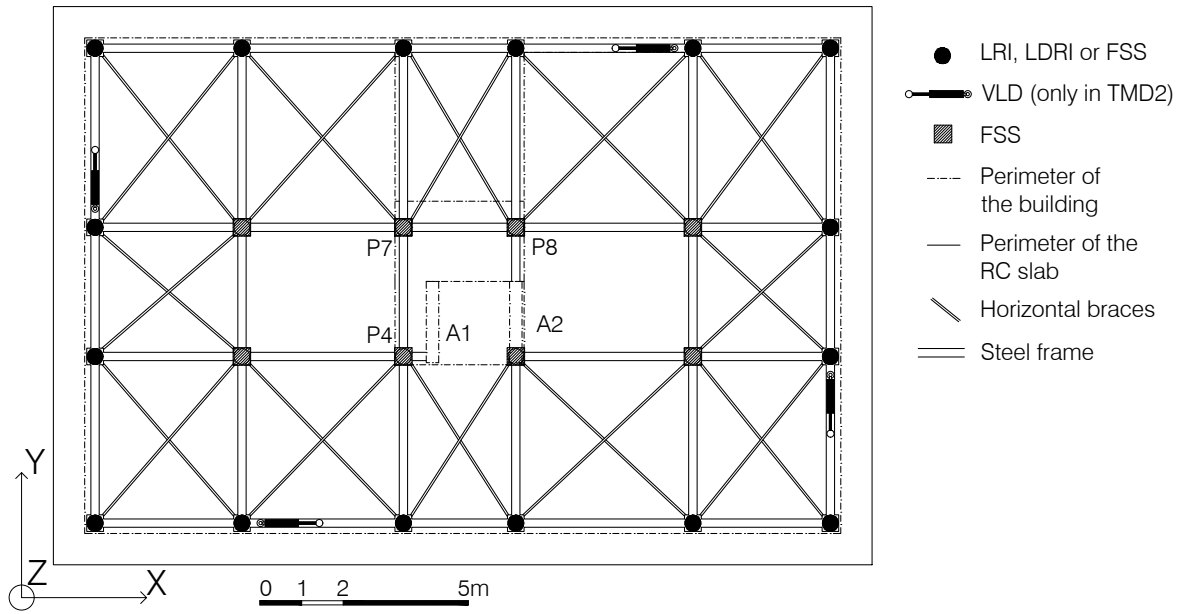


**Figure 7.** Top view of the steel structure supporting the TMD, and arrangement of dampers, isolators and sliders.

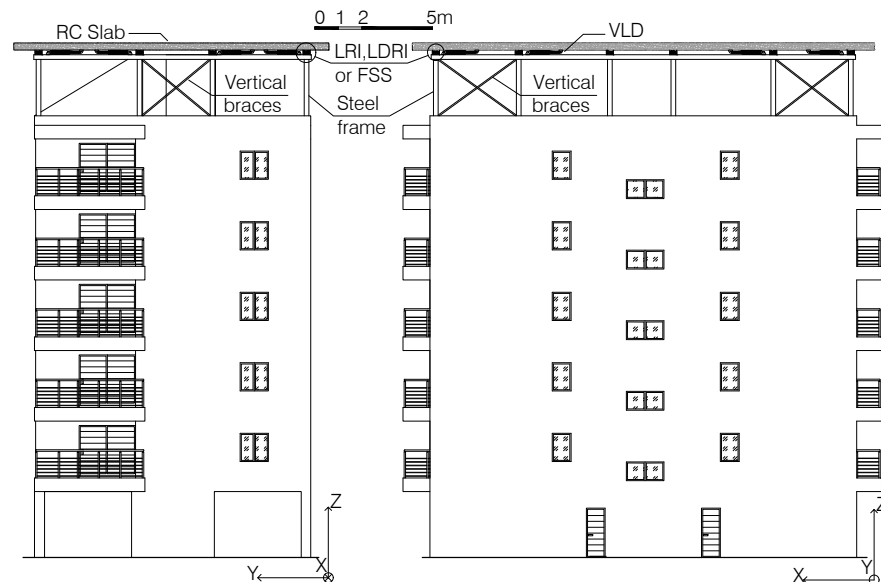


**Figure 8.** Elevation of the building equipped with the TMD in X direction on the left and Y direction on the right.

Since the horizontal stiffness and the energy dissipation contribution of the FSSs are negligible, to provide the TMD system with these properties, two solutions are proposed. In one solution (hereinafter referred to as TMD1), horizontal stiffness and damping are both provided by RIs, which are placed on the perimeter of the steel structure (Figure 7).



In the other solution (referred to as TMD2), horizontal stiffness is provided by LDRIs and damping by VLDs, which are installed along the perimeter of the steel structure, as can be seen in Figures 7 and 8.

The construction of the TMD may follow these steps:

- Installation of metal anchors to connect the base of the steel frame columns to the top end of the RC columns and walls of the building;
- Assemblance of the steel frame with columns, beams and vertical and horizontal braces;
- Installation of the FSSs, LRIs (in TMD1) and LDRIs (in TMD2) at the intersection nodes of beams, on the top of the steel frame, in the stairwell and in the elevator shaft, using steel plates to support them, if necessary. A way of access must be guaranteed for maintenance and to inspect and replace the isolation devices;
- Positioning of the form and the steel reinforcement for the concrete slab on the top of the steel frame and pouring of the concrete. A slight slope for water collection is required;
- In TMD2, VLDs can be installed after the curing of the concrete, connecting one end to a beam of the steel frame and the other to the under-surface of the RC slab, far enough away from the isolators to let them deform without making contact with the VLDs.

In both solutions, the design of the TMD is performed according to the analytical method described by Christopoulos in [5]. In this method, the building structure is modeled through a single-degree-of-freedom (DOF) system of mass  $M$  and stiffness  $K$ , connected to the TMD mass,  $m$ , by a linear elastic spring of stiffness  $k$  and a linear viscous damper with viscous coefficient  $c$ , disposed in parallel, as shown in Figure 9. Therefore, the TMD behavior is completely described by the three parameters  $m$ ,  $k$  and  $c$ .

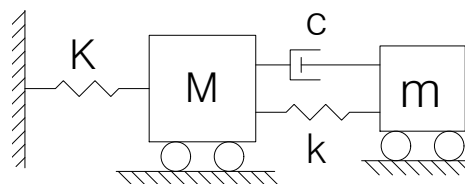


**Figure 9.** Schematization of the structure of the TMD system.

The dynamics of the two-DOF system in Figure 9 when it is subjected to acceleration  $a(t)$  at the base are described by Equations (1) and (2).

$$Ma_{OB}(t) + c[v_{OB}(t) - v_{TMD}(t)] + Kd_{OB}(t) + k[d_{OB}(t) - d_{TMD}(t)] = -Ma(t) \quad (1)$$

$$ma_{TMD}(t) + c[v_{TMD}(t) - v_{OB}(t)] + k[d_{TMD}(t) - d_{OB}(t)] = -ma(t) \quad (2)$$

where  $a_{OB}$ ,  $a_{OB}$ ,  $v_{OB}$ ,  $v_{TMD}$ ,  $d_{OB}$  and  $d_{TMD}$  are the accelerations, velocities and displacements of OB and TMD, respectively, relative to the base.

The design method is based on the minimization of the building displacements caused by a random acceleration time history acting at its base. This criterion allows the limitation of the stress demand on structural members and the avoidance of damage to non-structural elements.

The design is carried out independently for motion along the  $X$  and  $Y$  directions. The TMD parameters obtained for each direction may be different due to the different properties (periods and participating mass ratios) of the main vibration modes along the main directions. The periods and the participating mass ratios of the main translational modes of the building considered in the case study are similar. Hence, the TMD parameters are calculated on the basis of the mode with the higher participating mass ratio. Otherwise, a TMD solution providing different stiffness and damping along the main directions of the building would have to be considered.

The determination of the TMD parameters  $m$ ,  $k$  and  $c$  is divided into the following steps:



1. Definition of the mass ratio  $\mu$  between the TMD mass,  $m$ , and the effective mass of the main vibration mode of the building without the TMD,  $M_i$ . In general, the choice of  $m$  has to be made taking into account the bearing capacity of the structural members. In this case study, the structure can easily support, at ULS, an additional vertical load up to about 500% of the total mass of the building. In order to optimize the choice of  $m$ , the design procedure proposed by Luft [44] is used herein. In this procedure, the mass ratio is determined as

$$\mu = 16(\zeta_{eq} - 0.8\zeta_i)^2 \tag{3}$$

where  $\zeta_i$  is the viscous damping factor of the  $i$ -th vibration mode of period  $T_i$  and the participating mass ratio  $\alpha_i$ , and  $\zeta_{eq}$  is the damping factor of the acceleration and displacement spectra,  $S_A$  and  $S_D$ , respectively.  $\zeta_{eq}$  is determined so that the following inequalities are satisfied:

$$a_{max} \geq \alpha_i S_A(T_i, \zeta_{eq}) \tag{4}$$

$$d_{max} \geq \alpha_i S_D(T_i, \zeta_{eq}). \tag{5}$$

In (4) and (5),  $a_{max}$  and  $d_{max}$  are the target maximum acceleration and displacement at the top of the building, respectively, that can be borne without damage by the structural members. The values of  $a_{max}$  and  $d_{max}$  are determined by scaling the amplitude of the accelerograms.

2. Calculation of the frequency ratio,  $f$ , between the frequencies of the TMD and of the structure with the following equation

$$f = \frac{\sqrt{1 - \frac{\mu}{2}}}{1 + \mu} \tag{6}$$

and then the TMD stiffness,  $k$ ,

$$k = m\Omega_i^2 f^2 \tag{7}$$

where  $\Omega_i = \sqrt{\frac{K_i}{M_i}}$  is the frequency of the  $i$ -th vibration mode of the building.

3. Calculation of the damping factor,  $\zeta$ , and the viscous damping coefficient  $c$  of the TMD with the following equations:

$$\zeta = \sqrt{\frac{\mu(1 - \frac{\mu}{4})}{4(1 + \mu)(1 - \frac{\mu}{2})}} \tag{8}$$

$$c = 2\zeta\omega m \tag{9}$$

where  $\omega = \sqrt{\frac{k}{m}}$  is the TMD's natural frequency.

The values of  $k$  and  $\zeta$  are then used in the design of isolators and dampers.

After the definition of these parameters, the design of the TMD is completed by the implementation of the FEM of the building and the performance of its analysis. The choice of the model input parameters could be improved by means of on-site experimental dynamic tests on the existing building in order to obtain information about the building's vibration modes. This information could be used to calibrate the FE model. In this way, the FEM-based approach to designing the TMD would better take into account the real behavior of the building. Another possibility to improve the design of the TMD is to realize a simple to-scale experimental dynamic test of a two-DOF system, such as the one in Figure 9, where the two carts may be moved by a vibration table or an actuator, which can apply an accelerogram to their base. The mass  $M$  should represent the building mass activated by the main vibration mode, and  $K$  the corresponding stiffness. Different values

should be chosen for the mass, the damping and the stiffness of the TMD to select the best combination that minimizes the force acting on the mass  $M$ . This force can be measured through a load cell.

In both cases, a direct-integration non-linear analysis should be conducted to assess the real behavior of the building with TMD.

### 3.1. TMD with RIs (TMD1)

In the first proposed solution, RIs are employed to provide the TMD with both stiffness and damping. The RI damping ratio,  $\zeta_{is}$ , usually ranges between 10% and 15%. The use of lead-rubber isolators (LRIs) can be considered when a higher damping coefficient is required, up to 35%.

To implement RIs in the FEM of the building, the non-linear link element called ‘Rubber Isolator’ is used. This element has a bilinear force–displacement (F-d) relationship, like the one shown in Figure 10. The first branch of the diagram, of slope  $k_1$ , describes the isolator behavior up to the yielding point of coordinates  $(d_1, F_1)$ , while the second branch, with slope  $k_2$ , describes the post-yielding behavior up to the maximum force  $F_2$  and the maximum displacement  $d_2$ .  $k_{eq}$  is the secant stiffness corresponding to the displacement that the RI undergoes.

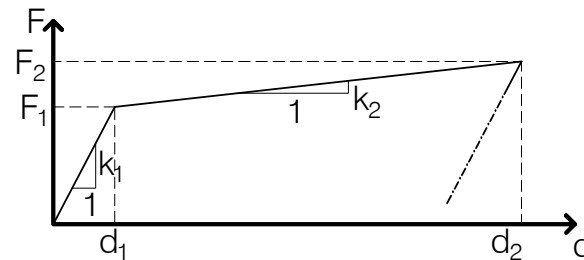


**Figure 10.** Bilinear force–displacement relationship of the ‘Rubber Isolator’ element.

The isolators’ design consists of choosing the number of devices and of determining their stiffness  $k_{eq}$  and equivalent damping factor  $\zeta_{is}$  through the design method described above. In particular,  $k_{eq}$  is obtained by dividing the value of  $k$  obtained from Equation (7) by the number of isolators, and  $\zeta_{is}$  coincides with the value of  $\zeta$  calculated with Equation (8). Then, the values of  $k_1$ ,  $F_1$  and  $k_2$  are computed with the formulas provided by FEMA [45].

### 3.2. TMD with LDRIs and VLDs (TMD2)

In addition to the FSSs, the second solution employs LDRIs and VLDs to provide the TMD with horizontal stiffness and damping, respectively.

LDRIs are composed of layers of natural rubber (without the usual additives, such as carbon black) alternating with steel shims. Since they have a damping factor of about 2%, in the FEM of the building, LDRIs are modeled through linear elastic springs of stiffness  $k_{LDRI}$ . Conversely, the non-linear behavior of VLDs is modeled in SAP2000 through the non-linear link ‘Damper - Bilinear’, in which a linear elastic spring of stiffness  $k_{VLD}$  and a dashpot are connected in series. The force in the dashpot is directly proportional to the relative velocity  $v$  of its ends through a damping coefficient  $c_{VLD}$  up to the maximum force  $F_{max}$ , as shown in Figure 11. The values of  $F_{max}$  and  $k_{VLD}$  are provided by the manufacturers of the device.

The value of  $k_{LDRI}$  is calculated by dividing  $k$  (from Equation (7)) by the number of LDRIs, while the value of  $c_{VLD}$  is calculated dividing  $c$  (from Equation (9)) by the number of VLDs.

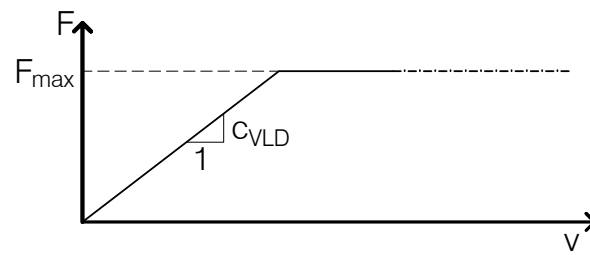


Figure 11. Bilinear force–velocity relationship of the ‘Damper–Bilinear’ element.

#### 4. Results

The design of the TMD is performed with the aim of changing the building’s structural behavior under SLV seismic actions from dissipative to non-dissipative. This aim is set to avoid damages to structural and non-structural elements at the SLV in order to eliminate costs for the building’s reparation. In regards to structural elements, damage is considered as the exceeding of the elements’ yield strength.

It is also fundamental to avoid TMD detuning. Actually, plasticization of structural members induces a modification of the building stiffness and vibrational modes, thus changing the building properties considered in the design process. According to [41], the structure’s behavior is non-dissipative if its members work in the so-called ‘substantially elastic field’.

The internal forces in the isolated structure are divided by a factor of 1.5, as allowed by the Italian Code [41] and the Eurocode [46]. For all vertical structural members, strength verifications are carried out at the base (0.00 m), at the top of the building (18.30 m) and at the level where the walls’ longitudinal reinforcements are reduced (12.30 m).

The properties of TMD1 and TMD2 derived from the design process are presented. The effects of TMD1 and TMD2 on the building’s modal behavior, strength verifications and energy dissipation are also provided. Results obtained for the building with TMD1 and TMD2 are compared with those of the OB and with those of the building seismically protected by a base isolation system (BIS).

##### 4.1. Properties of TMD1 and TMD2

As discussed in Section 3, the TMD design is based on the main vibration modes of the building. Since the installation of the TMD on the building’s rooftop requires the steel frame structure described in Section 3, the vibration modes to consider are those of the OB with the steel structure on the top (OBS). Table 4 shows the periods and the participating mass ratios of the most significant modes of the OBS.

Table 4. Periods and mass participating ratios of the most significant modes of OBS.

Mode <i>i</i>	<i>T<sub>i</sub></i>	$\alpha_{i,X}$	$\alpha_{i,Y}$	$\alpha_{i,Rz}$	$\Sigma \alpha_{i,X}$	$\Sigma \alpha_{i,Y}$	$\Sigma \alpha_{i,Rz}$
1	0.41 s	66.3%	0.2%	1.0%	66.3%	0.2%	1.0%
2	0.40 s	0.2%	68.3%	0.0%	66.5%	68.5%	1.0%
3	0.35 s	1.0%	0.0%	66.2%	67.5%	68.6%	67.3%
4	0.09 s	0.0%	18.4%	0.0%	67.5%	87.0%	67.3%
5	0.09 s	19.5%	0.0%	0.1%	87.1%	87.0%	67.5%
6	0.08 s	0.1%	0.0%	19.2%	87.2%	87.0%	86.8%

From Table 4, it can be seen that the first two modes are translational in the *X* and *Y* directions, respectively, and the third is rotational. These three modes have similar periods, ranging between 0.35 s and 0.41 s, and very similar participating mass ratios in the main direction, varying between 62.2 % and 68.3%. The remaining modes have lower periods, ranging between 0.08 s and 0.09 s. The modes of the OBS are practically identical to those of the OB (Table 3).

The design method requires that the values of  $a_{max}$  and  $d_{max}$  be fixed. In order to maintain the structural members in the elastic field and to avoid damage to masonry infill

panels under the seismic actions at the SLV, the values  $a_{max} = 3.26 \text{ m/s}^2$  and  $d_{max} = 0.011 \text{ m}$  were taken. These values lead to a mass ratio equal to 0.51. As the effective mass of mode 2,  $M_2$  equal to  $1183 \text{ t}$ , an RC slab thickness of  $z_{TMD}$  equal to  $0.90 \text{ m}$  is derived. If the TMD design was made taking different values of  $a_{max}$  and  $d_{max}$  in the X and Y directions, the values of  $a_{max}$  and  $d_{max}$  to take in the X direction would be  $3.50 \text{ m/s}^2$  and  $0.012 \text{ m}$ , respectively, which would lead to  $\mu = 0.38$ . Consequently, with  $M_1 = 1148 \text{ t}$ , a thickness of the RC slab equal to  $0.65 \text{ m}$  would be obtained.

From the values of  $k$  and  $\zeta$ , the number and characteristics of LRIs, for TMD1, and those of LDRIs and VLDs, for TMD2, can be determined. Then, the strength verifications of structural members are made, and the maximum values of the flexural demand over capacity ratio  $\frac{M_{Ed}}{M_{Rd}},_{max}$  equal to 1.45 for TMD1 and equal to 1.94 for TMD2 are found.

However, the values obtained for  $\mu$  and  $z_{TMD}$  are considered to be too large. Therefore, the performance of smaller TMDs is investigated. The trend of  $\frac{M_{Ed}}{M_{Rd}},_{max}$  obtained for TMD1 and TMD2 as  $\mu$  varies between 0 (OB) and 0.51 is shown in Figure 12.

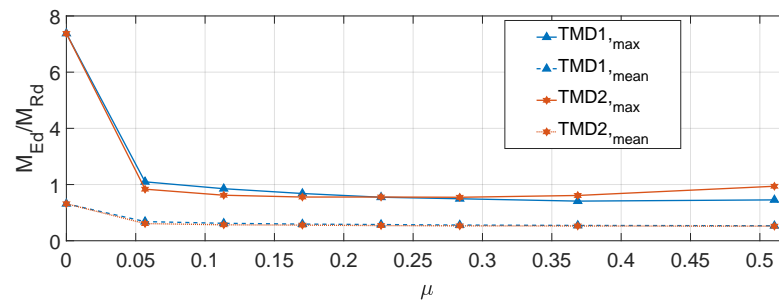


Figure 12. Trend of the maximum and mean values of the flexural demand over capacity ratios,  $\frac{M_{Ed}}{M_{Rd}},_{max}$  as a function of the mass ratio  $\mu$ .

In this figure, the mean values of the flexural demand over capacity ratios obtained for the two proposed solutions are also shown. From Figure 12, it can be seen that, in both solutions,  $\frac{M_{Ed}}{M_{Rd}},_{mean}$  decreases monotonically as  $\mu$  increases, passing from 1.3 for the OB to 0.53 for TMD1 and 0.52 for TMD2, but the decrease is negligible from  $\mu = 0.11$ . Moreover, from Figure 12, it can be observed that the designed TMDs do not lead to the minimum values of  $\frac{M_{Ed}}{M_{Rd}},_{max}$  as the minimum values are achieved with lower values of  $\mu$ , and in particular with  $\mu = 0.38$  for TMD1 and  $\mu = 0.28$  for TMD2. Therefore, a greater mass of the TMD does not mean better performance. Hence, the optimum thickness is defined on the basis of the percentage of not-satisfied verifications (PNV) of the structural members. The trend of PNV as a function of  $\mu$  obtained for the two solutions is shown in Figure 13.

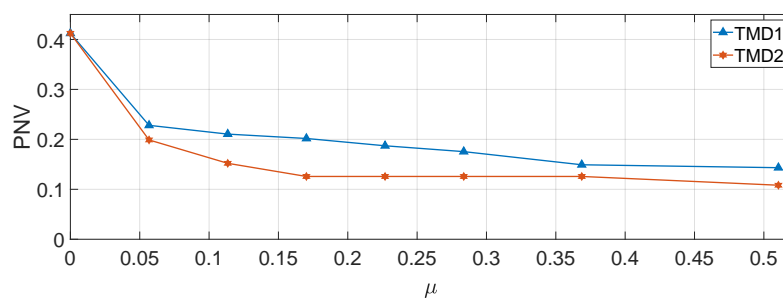


Figure 13. Percentage of not-satisfied verifications as a function of the mass ratio  $\mu$ .

From Figures 12 and 13, it can be observed that for both TMD solutions  $\mu = 0.2$  is already sufficient to largely reduce the flexural demand to structural members and the PNV. Mass ratios larger than 0.2 provide only a slight further reduction in the flexural demand

and the PNV. In particular, both solutions provide the best results for  $\mu > 0.35$ , but, also taking into account the  $\frac{M_{Ed}}{M_{Rd,max}}$  trend, the values  $\mu = 0.38$  for TMD1 and  $\mu = 0.17$  for TMD2 are considered optimal.

These values of  $\mu$  are obtained from the values of  $z_{TMD}$  reported in column (1) of Tables 5 and 6 for TMD1 and TMD, respectively. The parameters of the TMD calculated with Equations (6)–(9) are reported in column (2) of Table 5 for TMD1 and Table 6 for TMD2. Then, the properties of LRIs for TMD1 (in column (3) of Table 5) and those of VLDs and LDRIs for TMD2 (in columns (3) and (4) of Table 6, respectively) are determined.

**Table 5.** TMD1 design properties.

TMD1			
(1)	(2)	(3)	
RC slab properties	Design parameters from Equations (7) and (8)	LRIs properties	
$z_{TMD} = 0.65 \text{ m}$ $m = 435 \text{ t}$ $\mu = 0.38$	$f = 0.65$ $k = 43,976 \text{ kN/m}$ $\zeta = 27.7\%$	$n^o = 4$ $k_{eq} = 10,994 \text{ kN/m}$ $k_1 = 19,059 \text{ kN/m}$ $F_1 = 152 \text{ kN}$	$k_1 = 1787 \text{ kN/m}$ $d_1 = 0.008 \text{ m}$ $d_2 = 0.083 \text{ m}$ $F_2 = 287 \text{ kN}$

**Table 6.** TMD2 design properties.

TMD2			
(1)	(2)	(3)	(4)
RC slab properties	Design parameters from Equations (7) and (8)	VLDs properties	LDRIs properties
$z_{TMD} = 0.30 \text{ m}$ $m = 201 \text{ t}$ $\mu = 0.17$	$f = 0.82$ $k = 33,389 \text{ kN/m}$ $\zeta = 19.5\%$ $c = 1011 \text{ kNs/m}$	$n^o / \text{direction} = 2$ $k_{VLD} = 55,000 \text{ kN/m}$ $c_{VLD} = 506 \text{ kNs/m}$ $F_{max} = 200 \text{ kN}$	$n^o = 16$ $k_{LDRI} = 2087 \text{ kN/m}$

The position of LRIs and that of VLDs and LDRIs in the building plan are shown in Figures 14 and 15, respectively. The schematization of the simplified two-DOF structure-TMD systems are shown in Figure 16.

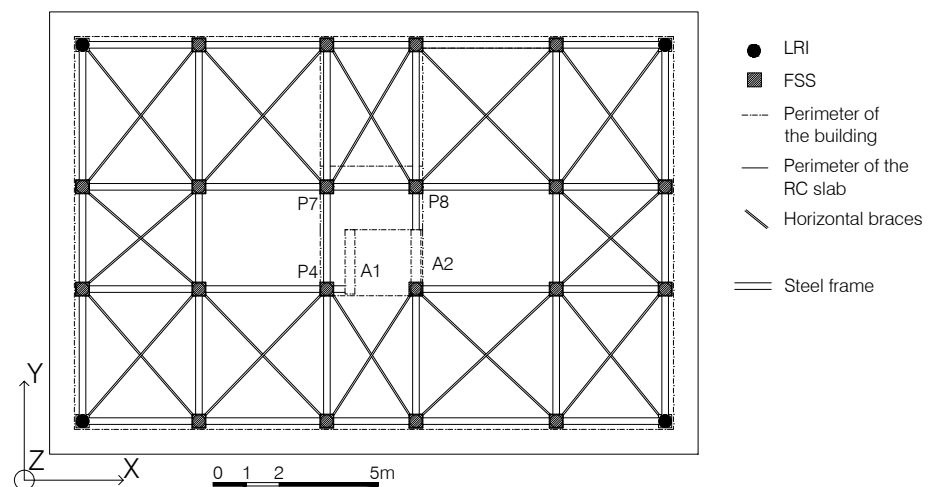


**Figure 14.** Top view of the steel structure supporting the TMD1 and arrangement of LRIs and FSSs.

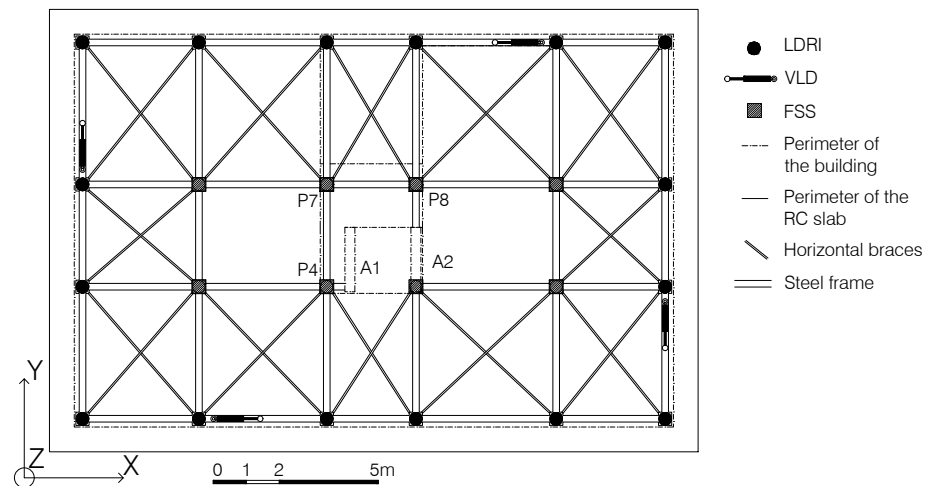


**Figure 15.** Top view of the steel structure supporting the TMD2 and arrangement of VLDs, LDRI and FSSs.

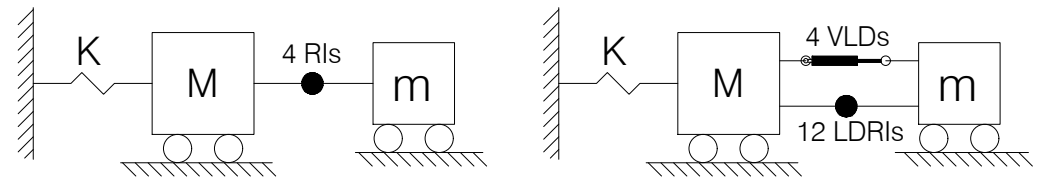


**Figure 16.** Schematization of the structure-TMD system for the building with TMD1 (left) and TMD2 (right).

TMD1 makes use of four LRIs placed at the corners of the steel structure, as shown in Figure 14, in order to maximize the TMD’s torsional stiffness.

In TMD2, due to the low shear modulus of LDRI, which is equal to 0.45 MPa, to provide the TMD with the design stiffness, 16 devices are required (Figure 15). Two VLDs in each main direction of the building are placed on the steel frame perimeter symmetrically with respect to the main axes of the building plan (Figure 15).

#### 4.2. Design of the Base Isolation System (BIS)

In addition to the seismic protection strategy based on the use of TMD, the strategy based on building seismic isolation is also considered. BIS is designed to increase the fundamental period  $T_1$  of the building up to the value  $T_{BIS}$  such that the corresponding spectral acceleration at the SLV,  $S_A(T_{BIS})$ , is equal to or lower than the spectral acceleration,  $S_A(T_1)$ , divided by the maximum value of  $\frac{M_{Ed}}{M_{Rd}}$ . For the OB,  $\frac{M_{Ed}}{M_{Rd}}_{max}$  is equal to 7.38. The stiffness of the BIS,  $k_{BIS}$ , is then determined from the total mass of the building,  $M$ , which is equal to 1740 t. For the considered case study,  $S_A(T_{BIS}) = 0.90 \text{ m/s}^2$ , which is attained for  $T_{BIS} = 2.90 \text{ s}$ . Consequently,  $k_{BIS} = 8175 \text{ kN/m}$  is obtained. To provide the BIS with this stiffness, eight RIs with the properties shown in Table 7 are used. The RIs are placed at the base of the walls lying on the building perimeter. At the base of the remaining structural elements, FSSs are installed. The layout of RIs and FSSs in the building plan is shown in Figure 17.

**Table 7.** Properties of RIs composing the BIS.

BIS			
$\zeta_{RI} = 12.5\%$	$k_1 = 7710 \text{ kN/m}$	$k_2 = 815 \text{ kN/m}$	$F_1 = 39 \text{ kN}$
$k_{eq,RI} = 1022 \text{ kN/m}$	$d_1 = 0.005 \text{ m}$	$d_2 = 0.167 \text{ m}$	$F_2 = 170 \text{ kN}$

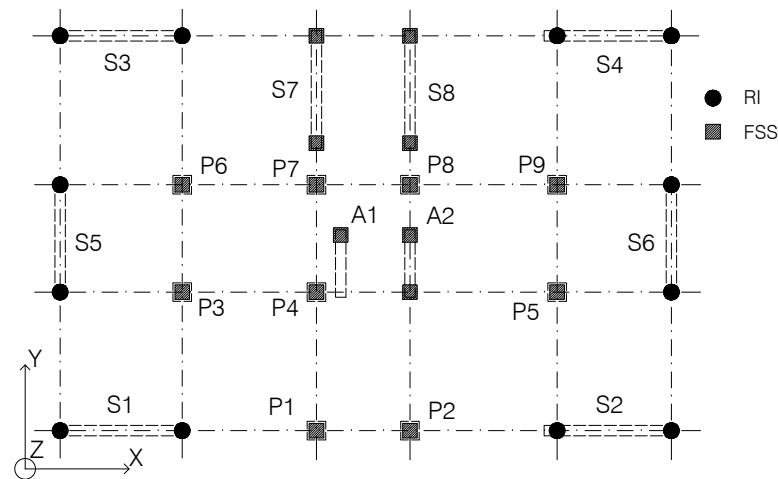


Figure 17. Layout of the base isolation system.

#### 4.3. Vibration Modes of the Building after the Interventions

The modal information of the building equipped with TMD1 is shown in Table 8.

Table 8. Periods and mass participating ratios of the most significant modes of the building equipped with TMD1.

Mode $i$	$T_i$	$\alpha_{i,X}$	$\alpha_{i,Y}$	$\alpha_{i,Rz}$	$\Sigma \alpha_{i,X}$	$\Sigma \alpha_{i,Y}$	$\Sigma \alpha_{i,Rz}$
1	0.62 s	0.0%	36.9%	0.0%	0.0%	36.9%	0.0%
2	0.61 s	36.7%	0.0%	0.0%	36.8%	36.9%	0.0%
3	0.47 s	0.0%	0.0%	48.7%	36.8%	36.9%	48.7%
4	0.31 s	0.1%	38.3%	0.0%	36.9%	75.2%	48.7%
5	0.31 s	37.8%	0.1%	0.0%	74.7%	75.3%	48.7%
6	0.24 s	0.1%	0.0%	26.2%	74.7%	75.3%	75.0%
7	0.08 s	0.0%	14.1%	0.0%	74.7%	89.4%	75.0%
8	0.08 s	14.9%	0.0%	0.1%	89.6%	89.4%	75.0%
9	0.07 s	0.1%	0.0%	14.2%	89.7%	89.4%	89.2%

From this table, it can be seen that the modes can be subdivided into three groups, each constituted by three modes: the first two translational in the X and Y directions, respectively, and the third rotational. The first group, composed of modes 1 to 3, is characterized by higher periods than those of OBS (Table 4), ranging from 0.62 s (mode 1) to 0.47 s (mode 3). The participating mass ratios of these modes range between 36.7% and 48.7%. The second group of modes, composed of modes 4, 5 and 6, is characterized by periods that are slightly lower than those of modes 1, 2 and 3 of the OBS and mass participating ratios that are about half, ranging between 26.2% (mode 6) and 38.3% (mode 4). The periods and mass participating ratios of the last group of modes (modes 7–9) are similar to those of modes 4–6 of the OBS. These modes are fundamentally those of the OBS, since the TMD does not participate in them.

Similarly to what was performed for the building equipped with TMD1, the modal properties of the building equipped with TMD2 are shown in Table 9.



**Table 9.** Periods and mass participating ratios of the most significant modes of the building equipped with TMD2.

Mode $i$	$T_i$	$\alpha_{i,X}$	$\alpha_{i,Y}$	$\alpha_{i,Rz}$	$\Sigma \alpha_{i,X}$	$\Sigma \alpha_{i,Y}$	$\Sigma \alpha_{i,Rz}$
1	0.58 s	0.1%	<u>36.2%</u>	0.0%	0.1%	36.2%	0.0%
2	0.57 s	<u>35.9%</u>	0.1%	0.0%	35.9%	36.3%	0.0%
3	0.49 s	0.0%	0.0%	<u>37.6%</u>	36.0%	36.3%	37.7%
4	0.32 s	0.2%	<u>37.5%</u>	0.0%	36.2%	73.8%	37.7%
5	0.32 s	<u>37.1%</u>	0.3%	0.0%	73.3%	74.1%	37.8%
6	0.27 s	0.2%	0.0%	<u>35.7%</u>	73.5%	74.1%	73.5%
7	0.09 s	0.0%	<u>14.8%</u>	0.0%	73.5%	88.9%	73.5%
8	0.08 s	<u>15.6%</u>	0.0%	0.1%	89.1%	88.9%	73.6%
9	0.07 s	0.1%	0.0%	<u>15.1%</u>	89.2%	88.9%	88.7%

From the comparison with Table 8, it can be observed that the effect of TMD2 on the vibration modes of the building is very similar to that of TMD1, since the periods and participating mass ratios of translational modes are almost identical. A slight difference emerges in rotational modes 3 and 6, whose participating mass ratios are, respectively, higher and lower than those of TMD1.

The modal information of the original building with the BIS is shown in Table 10.

**Table 10.** Periods and mass participating ratios of the most significant modes of the base-isolated building.

Mode $i$	$T_i$	$\alpha_{i,X}$	$\alpha_{i,Y}$	$\alpha_{i,Rz}$	$\Sigma \alpha_{i,X}$	$\Sigma \alpha_{i,Y}$	$\Sigma \alpha_{i,Rz}$
1	2.87 s	<u>99.9%</u>	0.0%	0.1%	99.9%	0.0%	0.1%
2	2.87 s	0.0%	<u>100.0%</u>	0.0%	99.9%	100.0%	0.1%
3	2.05 s	0.1%	0.0%	<u>99.9%</u>	100.0%	100.0%	100.0%

It can be seen that the dynamic behavior of the building is fully described by only three modes, which altogether provide participating mass ratios of 100% for each DOF of the building. The periods of the translational modes, equal to 2.87 s for modes 1 and 2, fall in the last branch of the acceleration site spectrum in Figure 5.

From the comparison of the modal analysis results of the OB (Table 4) with those of the building equipped with TMD1 (Table 8), TMD2 (Table 9) and BIS (Table 10), it can be noticed that all three interventions produce significant modifications of the building modes.

#### 4.4. Strength Verifications

The flexural demand over the capacity ratios for the OB and the building equipped with TMD1, TMD2 and BIS and their percentage variation from those of the OB are shown in Tables 11 and 12, respectively, for walls and columns.

Shear demand on structural members is always lower than their current capacity for the OB, and it is reduced in the building with TMD1, TMD2 and BIS. In particular, the shear demand at the base of the vertical members is reduced by at least 50% for the building equipped with TMD and 90% for the base-isolated building. Axial forces are also reduced by at least 60% and 90%, respectively.

**Table 11.** Flexural demand over capacity ratios for the walls of the OB and the building equipped with TMD1, TMD2 and BIS and percentage variation in the ratios with respect to those of the OB. Ratios greater than one are underlined; maximum values are in bold.

Wall Section	OB	TMD1		TMD2		BIS	
	$\frac{M_{Ed}}{M_{Rd}}$	$\frac{M_{Ed}}{M_{Rd}}$	$\Delta\%$	$\frac{M_{Ed}}{M_{Rd}}$	$\Delta\%$	$\frac{M_{Ed}}{M_{Rd}}$	$\Delta\%$
A01(0.0)	<u>2.86</u>	0.94	−67.1%	0.98	−65.8%	0.21	−92.7%
A01(12.3)	0.57	0.27	−52.2%	0.25	−55.9%	0.04	−92.4%
A01(18.3)	0.72	<u>1.01</u>	+41.2%	0.86	+20.5%	0.06	−91.1%
A02(0.0)	<b>7.38</b>	0.91	−87.6%	0.99	−86.6%	0.19	−97.4%
A02(12.3)	<u>1.30</u>	0.25	−80.5%	0.23	−77.2%	0.07	−94.4%
A02(18.3)	<u>1.34</u>	<u>1.16</u>	−17.1%	0.99	−28.7%	0.11	−91.9%
S01(0.0)	<u>3.37</u>	<u>1.33</u>	−60.5%	<u>1.42</u>	−58.0%	0.27	−92.1%
S01(12.3)	0.83	0.31	−62.2%	0.27	−64.4%	0.05	−94.6%
S01(18.3)	0.47	<u>1.28</u>	+172.4%	0.94	+100.8%	0.04	−91.2%
S02(0.0)	<u>3.42</u>	<u>1.31</u>	−61.8%	<u>1.36</u>	−60.3%	0.26	−92.4%
S02(12.3)	0.85	0.30	−64.7%	0.30	−64.7%	0.05	−94.0%
S02(18.3)	0.48	0.79	+63.7%	0.64	+33.7%	0.05	−90.2%
S03(0.0)	<u>3.59</u>	<b>1.40</b>	−61.0%	<u>1.44</u>	−59.9%	0.27	−92.4%
S03(12.3)	0.86	0.30	−64.9%	0.29	−66.7%	0.05	−94.4%
S03(18.3)	0.41	<u>1.26</u>	+209.9%	0.97	+137.8%	0.03	−92.9%
S04(0.0)	<u>3.63</u>	<u>1.38</u>	−62.0%	<u>1.42</u>	−61.0%	<b>0.28</b>	−92.4%
S04(12.3)	0.88	0.30	−65.6%	0.28	−67.9%	0.05	−94.3%
S04(18.3)	0.40	0.69	+72.9%	0.63	+56.7%	0.03	−91.5%
S05(0.0)	<u>3.07</u>	<u>1.27</u>	−58.7%	<u>1.34</u>	−56.3%	0.24	−92.3%
S05(12.3)	0.70	0.34	−51.9%	0.30	−57.4%	0.04	−94.6%
S05(18.3)	0.57	0.76	+33.7%	0.56	−1.9%	0.04	−92.8%
S06(0.0)	<u>3.09</u>	<u>1.27</u>	−58.9%	<u>1.37</u>	−55.7%	0.25	−91.9%
S06(12.3)	0.65	0.35	−45.6%	0.31	−52.4%	0.04	−93.2%
S06(18.3)	0.60	0.74	+21.9%	0.57	−5.6%	0.05	−92.3%
S07(0.0)	<u>5.48</u>	<b>1.40</b>	−74.4%	<b>1.56</b>	−71.6%	0.26	−95.3%
S07(12.3)	0.89	0.30	−66.6%	0.34	−62.2%	0.05	−94.6%
S07(18.3)	0.74	0.70	−6.1%	0.66	−11.1%	0.05	−93.7%
S08(0.0)	<u>6.70</u>	<b>1.40</b>	−79.1%	<u>1.55</u>	−76.8%	0.26	−96.1%
S08(12.3)	<u>1.04</u>	0.29	−72.1%	0.33	−68.5%	0.05	−95.4%
S08(18.3)	0.78	0.74	−5.3%	0.68	−12.4%	0.04	−94.6%

**Table 12.** Flexural demand over capacity ratios for the columns of the OB and the building equipped with TMD1, TMD2 and BIS and percentage variation in the ratios with respect to those of the OB. Ratios greater than one are underlined, maximum values are in bold.

Column Section	OB	TMD1		TMD2		BIS	
	$\frac{M_{Ed}}{M_{Rd}}$	$\frac{M_{Ed}}{M_{Rd}}$	$\Delta\%$	$\frac{M_{Ed}}{M_{Rd}}$	$\Delta\%$	$\frac{M_{Ed}}{M_{Rd}}$	$\Delta\%$
P01(0.0)	0.83	0.34	−59.0%	0.35	−58.6%	0.06	−92.9%
P01(12.3)	0.73	0.21	−70.9%	0.25	−65.4%	0.05	−93.9%
P01(18.3)	<u>1.29</u>	0.44	−65.9%	0.48	−63.1%	0.08	−93.8%
P02(0.0)	0.91	0.33	−63.3%	0.34	−62.1%	0.06	−93.4%
P02(12.3)	0.82	0.20	−75.1%	0.25	−69.9%	0.05	−94.3%
P02(18.3)	<u>1.45</u>	0.47	−67.3%	0.51	−65.2%	0.09	−93.9%
P03(0.0)	0.80	0.33	−58.5%	0.33	−58.1%	0.06	−92.6%
P03(12.3)	0.90	0.25	−72.0%	0.30	−66.3%	0.06	−93.5%
P03(18.3)	<u>1.68</u>	0.42	−74.9%	0.47	−71.9%	0.11	−93.5%

Table 12. Cont.

Column Section	OB	TMD1		TMD2		BIS	
	$\frac{M_{Ed}}{M_{Rd}}$	$\frac{M_{Ed}}{M_{Rd}}$	$\Delta\%$	$\frac{M_{Ed}}{M_{Rd}}$	$\Delta\%$	$\frac{M_{Ed}}{M_{Rd}}$	$\Delta\%$
P04(0.0)	0.91	0.33	−63.9%	0.34	−63.1%	0.06	−93.2%
P04(12.3)	0.75	0.19	−74.8%	0.23	−68.9%	0.05	−93.3%
P04(18.3)	<u>1.38</u>	0.54	−59.0%	0.48	−63.6%	0.09	−92.9%
P05(0.0)	0.77	0.33	−57.5%	0.33	−56.3%	0.06	−92.3%
P05(12.3)	0.78	0.25	−67.3%	0.30	−61.4%	0.06	−92.6%
P05(18.3)	<u>1.49</u>	0.39	−73.6%	0.44	−70.2%	0.11	−92.6%
P06(0.0)	0.76	0.33	−56.3%	0.34	−55.3%	0.06	−92.5%
P06(12.3)	0.86	0.26	−70.3%	0.30	−64.9%	0.05	−94.2%
P06(18.3)	<u>1.63</u>	0.41	−74.6%	0.47	−71.4%	0.09	−94.3%
P07(0.0)	<u>7.31</u> <sup>1</sup>	0.49	−93.2%	0.52	−92.9%	0.08	−98.9%
P07(12.3)	<u>2.17</u>	0.60	−72.4%	0.73	−66.5%	0.10	−95.4%
P07(18.3)	<u>2.71</u>	<u>1.41</u>	−48.0%	<u>1.49</u>	−45.0%	0.16	−94.3%
P08(0.0)	<u>1.80</u>	0.46	−74.2%	0.49	−72.5%	0.08	−95.4%
P08(12.3)	<u>2.28</u>	0.69	−69.9%	0.82	−64.3%	0.14	−93.9%
P08(18.3)	<u>3.24</u>	<u>1.29</u>	−60.2%	<u>1.32</u>	−59.5%	<b>0.21</b>	−93.6%
P09(0.0)	0.84	0.33	−60.6%	0.34	−59.9%	0.06	−92.9%
P09(12.3)	0.94	0.25	−73.4%	0.31	−67.3%	0.06	−93.9%
P09(18.3)	<u>1.77</u>	0.37	−79.0%	0.46	−74.3%	0.11	−94.0%

<sup>1</sup> Tensile axial force at the base of column P07 is greater than its cross-section capacity in one of the three analyses conducted.

#### 4.5. Input and Dissipated Energies

The graphs of cumulative input and dissipated energies of the OB and of the building with TMD1, TMD2 and BIS obtained from one of the three non-linear analysis cases are shown in Figure 18.

The force–displacement diagrams in the X and Y directions of one LRI (TMD1) and one VLD (TMD2) are shown in Figures 19 and 20, respectively. Similarly, the force–displacement diagrams in the X and Y directions of one RI of the base-isolated building are shown in Figure 21.

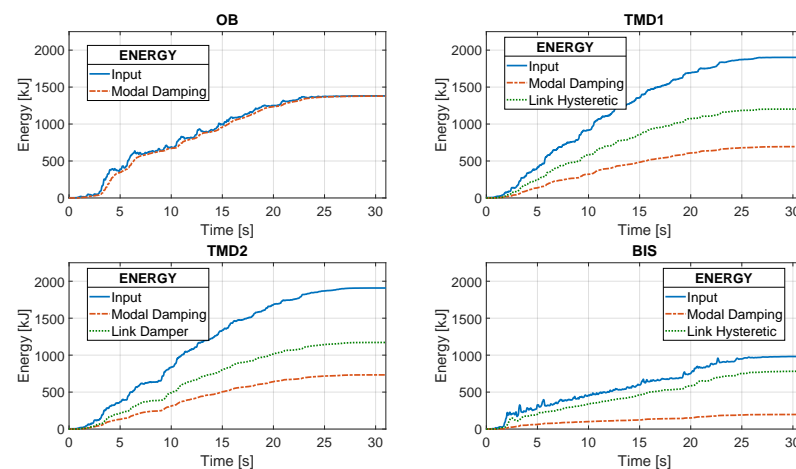
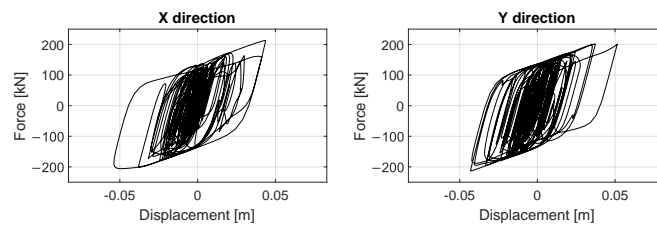
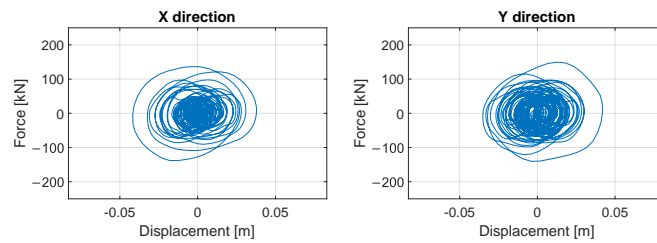


Figure 18. Cumulative input and dissipated energies for the OB and the building with TMD1, TMD2 and BIS.



**Figure 19.** Force–displacement diagrams along X and Y directions of one LRI for the building equipped with TMD1.



**Figure 20.** Force–displacement diagrams along X and Y directions of one VLD for the building equipped with TMD2.

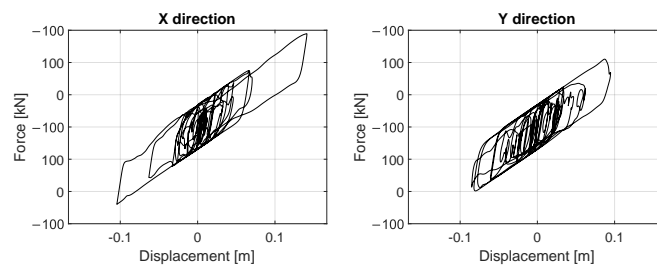


**Figure 21.** Force–displacement diagrams along X and Y directions of one RI for the building equipped with BIS.

#### 4.6. Maximum Accelerations

In Figure 22, the roof barycenter acceleration along the X direction of the OB and of the building with TMD1, TMD2 and BIS versus time graphs is shown. The peaks of maximum acceleration in each graph are highlighted with a red circle. The maximum amplitude of acceleration on the OB equals  $10.9 \text{ m/s}^2$ , and it can be observed that the installation of TMD1 and TMD2 reduces its value to  $7.4 \text{ m/s}^2$  and  $6.3 \text{ m/s}^2$ , respectively, while the base isolation system binds it below  $0.8 \text{ m/s}^2$ .

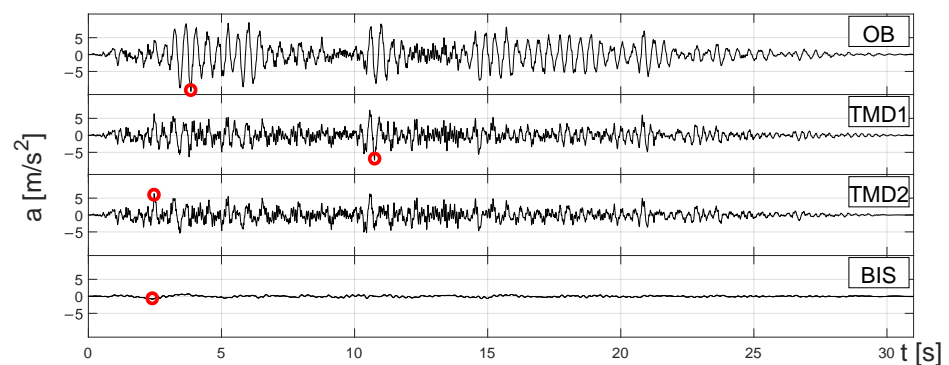


**Figure 22.** Acceleration–time graph of the barycenter of the building roof along X direction for all the considered configurations during one of the conducted analyses.

## 5. Discussion of Results

### 5.1. TMD Design Procedure

A high sensitivity of the formula proposed by Luft [44] to the maximum target displacement,  $d_{max}$ , of the building was observed. Due to this sensitivity, a high value of the mass ratio ( $\mu = 0.51$ ) was obtained. This is probably due to the fact that Luft's formula was derived for high-rise buildings, to which TMDs with a low mass ratio (i.e., with  $\mu \leq 0.10$ ) are usually applied. Then, the performance of lighter TMDs (i.e., with  $\mu \leq 0.51$ ) was investigated.

### 5.2. Building Vibration Modes

In Section 4.3, it was observed that the rotational modes 3 and 6 of the building equipped with TMD2 have participating mass ratios that are slightly different from those of modes 3 and 6 of the building with TMD1. This is due to the different arrangement in the building plan of LDRIs in TMD2 (Figure 15) with respect to LRIs in TMD1 (Figure 14), which induces a difference in the rotational stiffness.

In Figure 23, the acceleration spectrum for the considered building site with 5% and 27.7% damping is shown. From this figure, it can be seen that the spectral accelerations of the first three modes of the OB belong to the constant acceleration branch. The spectral acceleration of the first mode is indicated as OBa in Figure 23.

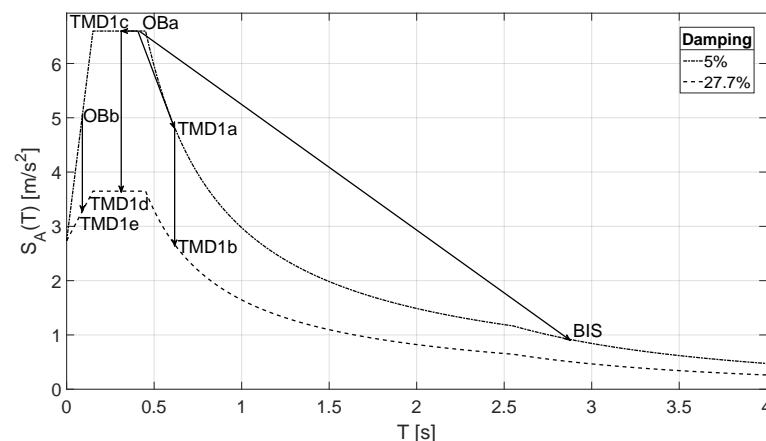


**Figure 23.** Reduction of the spectral accelerations of the modes with the most significant participating mass ratios in X direction for the building equipped with TMD1.

As observed in Section 4.3, the first six modes of the building equipped with TMD1 have participating mass ratios similar to those of the building with TMD2. The periods of the first three are higher than those of the OB and involve lower spectral accelerations belonging to the constant velocity branch. Conversely, the periods of the other three modes are lower than those of the OB, but involve a spectral acceleration that is still on the plateau. To show the effect of periods' change on spectral accelerations due to TMD, the spectral accelerations for  $\xi = 5\%$  of modes 1 and 4 of the building with TMD1 are indicated in Figure 23 and labeled as TMDa and TMDc, respectively. The damping provided by TMD further reduces spectral accelerations, thus moving points TMDa and TMDc to points TMDb and TMDd, respectively (see Figure 23).

The last three modes of the OB do not change remarkably with the installation of the TMD, but their spectral accelerations are reduced due to damping. Thus, it can be gathered that higher frequency modes only benefit from the TMD by damping and not by tuning. To show this, the spectral acceleration of mode 4 of the OB and that of the corresponding mode of the building with TMD1 (mode 7) are indicated by points OBb and TMDe in Figure 23, respectively.

From Figure 23, it can be seen that, thanks to the intervention with TMD1, the whole building is subjected to spectral accelerations ranging between 2.66 and 3.64 m/s<sup>2</sup>, which are lower than those of the OB (5.07–6.60 m/s<sup>2</sup>). As a consequence, internal forces in structural members due to seismic action are considerably reduced.

As for the base-isolated building, from Figure 23, it can be seen that the spectral acceleration of the first mode (point BIS) belongs to the spectrum constant displacement branch, which is characterized by the lowest accelerations. As a consequence, very low seismic forces arise in the building. Damping brought by RIs has very little relevance to spectral acceleration reduction.

### 5.3. Strength Verifications

From Tables 11 and 12, it can be seen that both TMDs remarkably improve flexural verifications since  $\frac{M_{Ed}}{M_{Rd}}$  ratios are significantly reduced for all structural members that have, in the OB,  $\frac{M_{Ed}}{M_{Rd}} > 1$ . However, the flexural demand on walls S01–S08, which counteract most of the seismic forces arising in the structure, is still greater than their capacity. Hence, the structure would be damaged by earthquakes with magnitudes the same as those considered. The missing gap could be reduced by using a more advanced design method for the TMD and increasing the reinforcements in the vertical members. Anyway, the flexural demand reduction is high, exceeding, in some cases, 70%.

From Tables 11 and 12, it can also be observed that  $\frac{M_{Ed}}{M_{Rd}}$  ratios increase at the top of almost all the walls due to the forces incurred by the TMD.  $\frac{M_{Ed}}{M_{Rd}}$  ratios and the PNV for the building equipped with TMD1 are very similar to those of the building equipped with TMD2. Thus, it can be said that the two proposed solutions, based on the use of TMD, are equally effective in reducing structural damage caused by seismic actions. The TMD2 should be preferred because the quantity of concrete required to make the RC slab is less than half of that required in TMD1. On the basis of the above, it can be concluded that the method adopted for the TMD design, though it is based on simple expressions, leads to remarkable results.

### 5.4. Input and Dissipated Energy

From Figure 18, it is seen that the OB dissipates all the input energy by modal damping. In reality, part of the input energy would also be dissipated by flexural plastic hinges forming at structural members ends, which have not been modeled in the FEM of the building. The effectiveness of both TMD solutions is also proven by the energy–time graphs shown in Figure 18. Actually, TMD1 and TMD2, despite inducing an increase in the total input energy, halve the energy dissipated by modal damping. From Figures 19 and 20, it can be seen that the mean force and the relative displacements are similar for the devices of TMD1 and TMD2. Thus, these devices dissipate similar energy amounts.

Among the intervention strategies considered in the presented case study, BIS is the most effective in reducing stresses arising in the structural members due to seismic actions. Indeed,  $\frac{M_{Ed}}{M_{Rd}}$  ratios are lower than one tenth of those of the OB, and the highest is 0.275 (see Tables 11 and 12). This is due to the fact that BIS reduces the input energy and dissipates most of it by RI's hysteretic cycles. Hence, the energy dissipated by the building through modal damping is reduced to at least one tenth of the OB. Despite the fact that the force–displacement cycles of RIs (Figure 21) are narrower than those of LRIs and VLDs (Figures 19 and 20), the energy dissipated by RIs is greater than that dissipated by LRIs and VLDs because RIs are more numerous than LRIs and VLDs.

TMD may also be a valid and efficient strategy for the retrofit of existing buildings as an alternative to dissipative braces [47,48] and base isolation [49,50], which often require interventions on the foundations and on the superstructure, making these solutions too expensive or technically unfeasible.

## 6. Conclusions

In this study, a tuned mass damper (TMD) was designed to be installed on the rooftop of a medium-rise building in order to change the building's behavior from dissipative to non-dissipative under seismic action. The application of the TMD was aimed at reducing stresses in structural members and floor displacement in order to avoid damage to structural and non-structural elements under strong earthquakes. Thereby, the building with TMD would not need reparation interventions after such earthquakes.

In the proposed solution, the mass of the TMD is made by an RC slab laying on flat surface sliders (FSSs) installed on the building rooftop. Two different solutions were proposed to provide the TMD with design stiffness and damping. In one solution (TMD1), stiffness and damping are both provided by lead rubber isolators (LRIs), while in the other solution (TMD2), stiffness and damping are provided by low-damping rubber isolators (LDRI) and viscous linear dampers (VLDs), respectively.

Starting from the TMD mass value obtained from the adopted design method, the optimal masses of TMD1 and TMD2 were 25% and 12% of the total mass of the building, respectively.

The proposed solutions led to very similar results. It was observed that the TMD significantly changes the main vibrational modes of the building, reducing the spectral accelerations. Consequently, a reduction in flexural and shear actions of at least 50% at the base of the walls and of at least 55% at the base of the columns was achieved. The flexural demand over capacity ratios were strongly reduced, bringing the maximum from 7.38 (OB) to 1.41 and 1.56 with TMD1 and TMD2, respectively. Based on this result, it can be concluded that the designed TMDs are effective in reducing the stresses in the structural elements of the considered medium-rise building, almost to the substantially elastic bound. Both TMDs involve an increase in the input energy, but most of it is dissipated through damping by TMD devices, hence halving the energy dissipated through modal damping by the building.

A base isolation system (BIS) was also designed to compare its effectiveness in reducing the stresses in the building's structural members with that of TMD1 and TMD2. BIS proved to be the most effective strategy, as expected, since it radically increased the periods of the building's vibration modes. This produces a reduction in the shear actions at the base of the building of at least 90%, leading the strength verifications of structural members to all be largely satisfied.

However, from the results obtained for the case study, it can be concluded that a TMD can be used for the retrofit of existing buildings as a valid alternative to base isolation when the latter is technically unfeasible.

**Author Contributions:** Conceptualization, methodology, M.P., L.M. and G.F.; software, validation, formal analysis, investigation, data curation, writing—original draft preparation, visualization, L.M.; writing—review and editing, L.M. and G.F.; resources, supervision, project administration, funding acquisition, M.P. All authors have read and agreed to the published version of the manuscript.

**Funding:** The research has been partially funded by: (1) the Italian Department of Civil Protection, within the framework of Executive Project DPCRe-LUIS 2022–2024; (2) the European Union Next-GenerationEU (PIANO NAZIONALE DI RIPRESA E RESILIENZA (PNRR)–MISSIONE 4 COMPONENTE 2, INVESTIMENTO 1.5–D.D. 1058 23/06/2022, ECS00000043), within the Interconnected Nord-Est Innovation Ecosystem (iNEST). This manuscript reflects only the authors' views and opinions, neither the European Union nor the European Commission can be considered responsible for them; (3) the strategic plan of University of Udine within the framework of the project "ESPeRT", whose support is greatly appreciated.

**Institutional Review Board Statement:** Not applicable.

**Informed Consent Statement:** Not applicable.

**Conflicts of Interest:** The authors declare no conflict of interest.



## References

1. Soto, M.G.; Adeli, H. Tuned Mass Dampers. *Arch. Comput. Methods Eng.* **2013**, *20*, 419–431. [[CrossRef](#)]
2. Yang, F. Vibration suppression of structures using tuned mass damper technology: A state-of-the-art review. *Struct. Multidisc. Optim.* **2022**, *27*, 7–8. [[CrossRef](#)]
3. Sadek, F.; Mohraz, B.; Taylor, A.W.; Chung, R.M. A method of estimating the parameters of tuned mass dampers for seismic applications. *Earthq. Eng. Struct. Dyn.* **1997**, *26*, 617–635. [[CrossRef](#)]
4. Chang, C.C. Mass dampers and their optimal designs for building vibration control. *Eng. Struct.* **1999**, *21*, 454–463. [[CrossRef](#)]
5. Christopoulos, C.; Filiatrault, A. *Principles of Passive Supplemental Damping and Seismic Isolation*; IUSS: Pavia, Italy, 2006; pp. 277–299.
6. Wang, P.C.; Kozin, F.; Amini, F. Vibration control of tall buildings. *Eng. Struct.* **1983**, *5*, 282–288. [[CrossRef](#)]
7. Joshi, A.S. Optimum parameters of multiple tuned mass dampers for base-excited damped systems. *J. Sound Vib.* **1997**, *202*, 657–667. [[CrossRef](#)]
8. Jangid, R.S. Optimum Multiple Tuned Mass Dampers for base-excited undamped system. *Earthq. Eng. Struct. Dyn.* **1999**, *28*, 1041–1049. [[CrossRef](#)]
9. Soto, M.G.; Adeli, H. Optimum tuning parameters of tuned mass dampers for vibration control of irregular highrise building structures. *J. Civ. Eng. Manag.* **2014**, *20*, 609–620.
10. Bagheri, S.; Rahmani-Dabbagh, V. Seismic response control with inelastic tuned mass dampers. *Eng. Struct.* **2018**, *172*, 712–722. [[CrossRef](#)]
11. Moutinho, C. An alternative methodology for designing tuned mass dampers to reduce seismic vibrations in building structures. *Earthq. Eng. Struct. Dyn.* **2012**, *41*, 2059–2073. [[CrossRef](#)]
12. Kamatchi, P.; Balaji Rao, K.; Sathish Kumar, K. Closed-Form Equations for Optimum Tuning Frequency and Damping Ratio of Tuned Mass Damper and Applicability for Site-Specific Earthquakes. *J. Inst. Eng.* **2020**, *101*, 19–26. [[CrossRef](#)]
13. Miranda, J.C. Discussion of system intrinsic parameters of tuned mass dampers used for seismic response reduction. *Struct. Control Health Monit.* **2016**, *23*, 349–368. [[CrossRef](#)]
14. Matta, E. Effectiveness of Tuned Mass Dampers against Ground Motion Pulses. *J. Struct. Eng.* **2013**, *139*, 188–198. [[CrossRef](#)]
15. Chung, L. Optimal design theories of tuned mass dampers with nonlinear viscous damping. *Earthq. Eng. Eng. Vib.* **2008**, *8*, 547–560. [[CrossRef](#)]
16. Reggio, A. Optimal energy-based seismic design of non-conventional Tuned Mass Damper (TMD) implemented via inter-story isolation. *Earthq. Eng. Struct. Dyn.* **2015**, *44*, 1623–1642. [[CrossRef](#)]
17. Sgobba, S.; Marano, G.C. Optimum design of linear tuned mass dampers for structures with nonlinear behaviour. *Mech. Syst. Signal Process.* **2010**, *24*, 1739–1755. [[CrossRef](#)]
18. Salvi, J.; Pioldi, F.; Rizzi, E. Optimum Tuned Mass Dampers under seismic Soil-Structure Interaction. *Soil Dyn. Earthq.* **2018**, *114*, 576–597. [[CrossRef](#)]
19. Tigli, O.F. Optimum vibration absorber (tuned mass damper) design for linear damped systems subjected to random loads. *J. Sound Vib.* **2018**, *331*, 3035–3049. [[CrossRef](#)]
20. Chey, M.; Kim, J. Parametric control of structural responses using an optimal passive tuned mass damper under stationary Gaussian white noise excitations. *Front. Struct. Civ. Eng.* **2012**, *6*, 267–280. [[CrossRef](#)]
21. Jia, F.; Jianwen, L. Performance degradation of tuned-mass-dampers arising from ignoring soilstructure interaction effects. *J. Soil Dyn. Earthq.* **2019**, *125*, 105701. [[CrossRef](#)]
22. Lucchini, A.; Greco, R.; Marano, G.C.; Monti, G. Robust Design of Tuned Mass Damper Systems for Seismic Protection of Multistory Buildings. *J. Struct. Eng.* **2014**, *140*, A4014009. [[CrossRef](#)]
23. Almazán, J.L.; Espinoza, G.; Aguirre, J.J. Torsional balance of asymmetric structures by means of tuned mass dampers. *Eng. Struct.* **2012**, *42*, 308–328. [[CrossRef](#)]
24. Espinoza, G.; Almazán, J.L.; Benedetti, F.; Jara, C. Torsional balance of nonlinear asymmetrical structures by means of a tuned mass damper. *Struct. Control Health Monit.* **2019**, *26*, e2442. [[CrossRef](#)]
25. Marano, G.C.; Greco, R.; Sgobba, S. A comparison between different robust optimum design approaches Application to tuned mass dampers. *Probabilistic Eng. Mech.* **2010**, *25*, 108–118. [[CrossRef](#)]
26. Bekdas, G.; Nigdeli, S.M. Estimating optimum parameters of tuned mass dampers using harmony search. *Eng. Struct.* **2011**, *33*, 2716–2723. [[CrossRef](#)]
27. Ozsariyildiz, S.; Bozer, A. Finding optimal parameters of tuned mass dampers. *Struct. Des. Tall Spec. Build.* **2015**, *24*, 461–475. [[CrossRef](#)]
28. Salvi, J.; Rizzi, E. Optimum tuning of Tuned Mass Dampers for frame structures under earthquake excitation. *Struct. Control Health Monit.* **2015**, *22*, 707–725. [[CrossRef](#)]
29. Chakraborty, S.; Roy, B.K. Reliability based optimum design of Tuned Mass Damper in seismic vibration control of structures with bounded uncertain parameters. *Probabilistic Eng. Mech.* **2011**, *26*, 215–221. [[CrossRef](#)]
30. Venanzi, I. Robust optimal design of tuned mass dampers for tall buildings with uncertain parameters. *Struct. Multidisc. Optim.* **2015**, *51*, 239–250. [[CrossRef](#)]
31. Yucel, M. Estimation of optimum tuned mass damper parameters via machine learning. *J. Build. Eng.* **2019**, *26*, 100847. [[CrossRef](#)]
32. Zhang, M. Tuned mass damper for self-excited vibration control: Optimization involving nonlinear aeroelastic effect. *J. Wind. Eng. Ind. Aerodyn.* **2022**, *220*, 104836. [[CrossRef](#)]

33. Hao, L.; He, H.; Tan, P.; Jin, K.; Liu, X. Performance and Efficiency Oriented Optimal Design of Tuned Inerter Damper for Seismic Response Control of Building Structures. *Int. J. Mech. Sci.* **2023**, *253*, 108394. [[CrossRef](#)]
34. Xiang, Y.; Tan, P.; He, H.; Yao, H.; Zheng, X.; Yang, K. A Novel Bi-directional Rail Variable Friction Pendulum-tuned Mass Damper (BRVFP-TMD). *Mech. Syst. Signal. Process.* **2023**, *197*, 110396. [[CrossRef](#)]
35. Elias, S.; Matsagar, V. Research developments in vibration control of structures using passive tuned mass dampers. *Annu. Rev. Control* **2017**, *44*, 129–156. [[CrossRef](#)]
36. Lin, G. Experimental study on seismic vibration control of an offshore wind turbine with TMD considering soil liquefaction effect. *Mar. Struct.* **2021**, *77*, 102961. [[CrossRef](#)]
37. Assatourians, A.; Mehrdoust, M. Seismic Upgrading of the 111 Serie Residential 10 Story R.C.Frame Buildings in Armenia, using Additional Isolated Upper Floor. In Proceedings of 9th National Congress on Civil Engineering, Mashhad, Iran, 10–11 May 2016.
38. Clemente, P.; Saitta, F.; Buffarini, G.; Bongiovanni, G. *Isolamento Sismico Edifici Esistenti—Criteri di Progetto e Applicazioni*; Grafill: Palermo, Italy, 2019; pp. 147–150.
39. Villaverde, R. Aseismic Roof Isolation System Feasibility Study with 13-Story Building. *J. Struct. Eng.* **2002**, *128*, 188–196. [[CrossRef](#)]
40. Johnson, J.G.; Pantelides, C.P.; Reaveley, L.D. Nonlinear rooftop tuned mass damper frame for the seismic retrofit of buildings. *Earthq. Eng. Struct. Dyn.* **2015**, *44*, 299–316. [[CrossRef](#)]
41. Ministero delle Infrastrutture e dei Trasporti. *DM 17 Gennaio 2018. Aggiornamento Delle “Norme Tecniche per le Costruzioni”*; Gazzetta Ufficiale: Rome, Italy, 2018; Volume 42. (In Italian)
42. Computers and Structures Inc. *SAP2000 Ultimate: Structural Analysis Program, Version 21.2.0*; Author SAP: Berkeley, CA, USA, 2021.
43. Gelfi, P. *SMQKE\_GR, Version 2.7*; University of Brescia: Brescia, Italy, 2012.
44. Luft, W. Optimal Tuned mass damper for buildings. *J. Struct. Div.* **1979**, *105*, 2765–2772. [[CrossRef](#)]
45. Federal Emergency Management Agency. *Prestandard and Commentary for the Sesimic Rehabilitation of Buildings*; Federal Emergency Management Agency: Washington, DC, USA, 2000.
46. *UNI EN 1998-1*; Eurocode 8: Design of Structures for Earthquake Resistance Part 1: General Rules, Seismic Actions and Rules for Buildings. European Committee for Standardization: Brussels, Belgium, 2005.
47. Frappa, G.; Pauletta, M. Seismic retrofitting of a reinforced concrete building with strongly different stiffness in the main directions. In Proceedings of 14th fib International PhD Symposium in Civil Engineering, Rome, Italy, 5–7 September 2022.
48. Miani, M.; Di Marco, C.; Frappa, G.; Pauletta, M. Effects of Dissipative Systems on the Seismic Behavior of Irregular Buildings—Two Case Studies. *Buildings* **2020**, *10*, 202. [[CrossRef](#)]
49. Pauletta, M.; Pinzano, F.; Frappa, G.; Russo, G. Tensile tests for the improvement of adhesion between rubber and steel layers in elastomeric isolators. *Appl. Sci.* **2020**, *10*, 8063. [[CrossRef](#)]
50. Pauletta, M. Method to design fiber-reinforced elastomeric isolators (U-FREIs) and Application. *Eng. Struc.* **2019**, *197*, 109366. [[CrossRef](#)]

**Disclaimer/Publisher’s Note:** The statements, opinions and data contained in all publications are solely those of the individual author(s) and contributor(s) and not of MDPI and/or the editor(s). MDPI and/or the editor(s) disclaim responsibility for any injury to people or property resulting from any ideas, methods, instructions or products referred to in the content.